A Journal of the Gesellschaft Deutscher Chemiker
Angewandte Chemie
GDCh
International Edition
www.angewandte.org

Accepted Article

Title: AgII-mediated electrocatalytic ambient CH4 functionalization inspired by HSAB theory

Authors: Danlei Xiang, Jesus A Iñiguez, Jiao Deng, Xun Guan, Antonio Martinez, and Chong Liu

To be cited as: *Angew. Chem. Int. Ed.* 10.1002/anie.202104217

Link to VoR: https://doi.org/10.1002/anie.202104217

WILEY-VCH

10.1002/anie.202104217

WILEY-VCH

RESEARCH ARTICLE

Ag^{II}-mediated electrocatalytic ambient CH_4 functionalization inspired by HSAB theory

Danlei Xiang,[a] Jesus A. Iñiguez,[a] Jiao Deng,[a] Xun Guan,[a] Antonio Martinez,[a] Chong Liu*[a,b]

[a] D. Xiang, J. A. Iñiguez, Dr. J. Deng, X. Guan, A. Martinez, Prof. Dr. C. Liu
Department of Chemistry and Biochemistry
University of California Los Angeles
Los Angeles, California 90095, United States
E-mail: chongliu@chem.ucla.edu

[b] Prof. Dr. C. Liu
California Nanoscience Institute
University of California Los Angeles
Los Angeles, California 90095, United States

Supporting information for this article is given via a link at the end of the document.

Abstract: Developing an efficient chemical transformation pathway of ambient CH_4 functionalization is an ongoing challenge and the key resides on the discovery of new catalytic systems. The hard-soft acid-base (HSAB) theory suggests that high-valent transition metals, as soft class (b) Lewis acids based on Pearson's classification, are suitable candidates for CH_4 activation due to methyl moiety's relatively low value of chemical hardness. While most of class (b) transition metals have been studied, divalent silver (Ag^{II}), possibly due to its reactive nature, is the only class (b) high-valent transition metal center that is yet reported to exhibit reactivities towards CH_4 activation. Inspired by such notion, here we report that electrochemically generated Ag^{II} metalloradical readily functionalizes CH_4 into methyl bisulfate (CH_3OSO_3H) at ambient conditions in 98% H_2SO_4. Mechanistic investigation experimentally unveils a low activation energy of 13.1 kcal•mol^{-1}, a high pseudo-first-order rate constant of CH_4 activation up to 2.8×10^3 h^{-1} at room temperature and a CH_4 pressure of 85 psi, and two competing reaction pathways preferable towards CH_4 activation over solvent oxidation. Reaction kinetic data suggest a Faradaic efficiency exceeding 99% beyond 180 psi CH_4 at room temperature for potential chemical production from widely distributed natural gas resources with minimal infrastructure reliance.

Introduction

Ambient CH_4 functionalization offers a route of chemical synthesis that taps on the vast, widely distributed natural gas resources while mitigating the environmentally unfriendly CH_4 emission into the atmosphere.[1] The key step in this process is the activation of CH_4's C−H bond at relatively low temperature and pressure, which demands a kinetically reactive species with a low activation barrier.[2] One approach in search of the desirable reactive species begins from the classic hard-soft acid-base (HSAB) theory, initially introduced by Ralph Pearson.[3] The theory introduces chemical hardness η as a measure of molecules' electrophilicity[4] and stability in the context of Lewis acid-base adduct. In a homolytic cleavage of CH_4, the transferred methyl moiety possesses relatively low chemical hardness (η = 4.87).[5] The softness of methyl moiety along with H atom (η = 6.42) involved in H-atom abstraction suggests that a soft, class (b) transition-metal Lewis acid of high valence and increased electrophilicity may be reactive towards CH_4 via either electrophilic activation[6] or a radical-based mechanism.[7] Consistently, many high-valent class (b) metals in the d-block of periodic table, including $Rh^{I, II}$,[8] $Pd^{II, III}$,[9] Ir^{III},[10] $Pt^{II, IV}$,[11] $Au^{I, III}$,[12] Hg^{II},[6b] have been reported for CH_4 activation (Figure 1a). Some of the borderline metals with intermediate chemical softness, including Mn^{III},[13] Co^{III},[13] $Ru^{IV, VIII}$,[14] $Os^{IV, VIII}$,[15] Tl^{III},[6c] and Pb^{IV},[6c, 13] are reactive towards CH_4, too. Yet there is one exception, silver (Ag). While monovalent Ag^{I} as a mild oxidant (η = 6.96; $E°$ = 0.80 V vs normal hydrogen electrode (NHE) for Ag^+ (*aq.*)/Ag (*s*))[5, 16] may not be oxidative enough to break the C−H bond in CH_4 ($E°$ = 0.59 V vs NHE for CH_3OH (*l*)/CH_4 (*g*)),[2b, 16] divalent Ag^{II} is similarly soft (η = 6.7)[5] and possesses a Ag^{II}/Ag^{I} redox potential ($E°$ = ~2.5 V vs NHE for Ag^{II}/Ag^{I} in 98% H_2SO_4)[17] comparable to other reported CH_4-activation catalysts.[2a, 2b, 9b] Therefore, it is intriguing that divalent Ag^{II} has not been known for CH_4 activation despite the reported Ag^{II}-based reactivities on much weaker C−H bonds in organic synthesis.[18] The d^9 electronic configuration of Ag^{II} not only renders it a metalloradical, but also introduces the Jahn-Teller effect in an O_h ligand field that elongates the ligand bond in the axial position (Figure 1b).[19] Such weakly bound axial ligands and Ag^{II}'s likely radical nature may offer an opportunity for substrate binding and CH_4 activation in a radical-based activation pathway with low reaction barrier, leading to our hypothesis that Ag^{II}, once continuously generated, may serve as the active species towards ambient CH_4 functionalization catalytically.

Our strategy of investigating Ag^{II} as a potential active species towards CH_4 activation includes continuous electro-generation of reactive Ag^{II} species in an inert solvent environment (Figure 1c). Electrochemistry offers a viable and clean route of creating reactive intermediates for synthesis including C−H activation.[20] Such a strategy has enabled our previous discovery of electrocatalytic CH_4 functionalization with vanadium-oxo dimer as the homogeneous catalysts at ambient temperature and pressure.[2a] Similarly, the strategy of electrochemical catalysis can be also applied for the generation of Ag^{II} intermediate, which circumvents the instability of Ag^{II} and establishes an electrocatalytic cycle mediated by the Ag^{II}/Ag^{I} redox couple (Figure 1c). We also sought to choose a weakly bound solvation environment as a model system that offers labile binding sites for substrate activation, supports the radical nature of Ag^{II} in a possible radical-based mechanism, and mitigates side reactions of solvent oxidation due to Ag^{II}'s reactive nature. Such

10.1002/anie.202104217

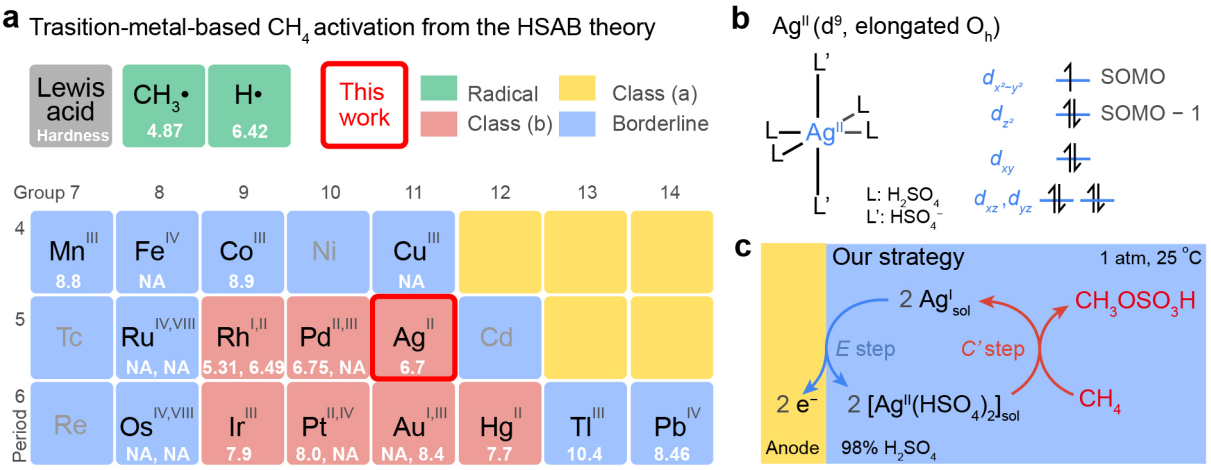

Figure 1. a) Transition metals reported for direct C−H activation of homogeneous CH_4 functionalization.[2b] The values of chemical hardness (η) are tabulated for the elements' respective oxidation states.[5] NA, not available. b) Schematics of the frontier orbitals and structure of a proposed Ag^{II} metalloradical in 98% H_2SO_4. L and L', ligands; SOMO, Singly Occupied Molecular Orbital. c) The strategy of an electrocatalytic CH_4 activation in this work.

consideration leads to the choice of 98% H_2SO_4, which not only minimizes possible water oxidation reaction due to its oxidative stability[2a, 2b] but also can stabilize Ag^{II} compound at 20 ºC.[21] The electron-withdrawing bisulfate ligand bound to Ag^{II} in 98% H_2SO_4 is postulated to provide access to CH_4 activation in the elongated axial position,[19a] maximize the radical nature on metal center due to spin localization,[19b] and simplify product detection by mitigating the additional oxidation with the formation of methyl bisulfate (CH_3OSO_3H) after a presumed two-electron oxidation. Such favorable features in conjunction with our expertise in electrochemical CH_4 activation[2a, 22] constitute our motivation for exploring a Ag^{II}-mediated electrocatalytic CH_4 functionalization in 98% H_2SO_4 inspired by the HSAB theory.

Here we present our demonstration of Ag^{II}-mediated electrocatalytic CH_4 activation in 98% H_2SO_4 at ambient conditions. We found that electrochemically generated Ag^{II} intermediate is capable of activating CH_4 and yielding CH_3OSO_3H with minimal side reactions at room temperature and ambient pressure. The CH_4-activation reactivity, measured as the partial current density of CH_3OSO_3H formation j_{CH4}, is systematically studied as a function of the applied electrochemical potential (E), duration of electrolysis (t), the concentration of pre-catalyst Ag^{I} (c_{Ag}), temperature (T), and the partial pressure of CH_4 (p_{CH4}) up to 125 psi. The results support the scheme of electrocatalysis for CH_4 functionalization mediated by Ag^{II} in an *EC'* mechanism[23] (Figure 1c), in which the electrochemically generated Ag^{II} undergoes a turnover-limiting CH_4-activating step with low activation energy (13.1 kcal•mol^{-1}), high pseudo-first-order rate constant (k_{obs}) of 2.8×10^3 h^{-1} (p_{CH4} = 85 psi), and a high turnover number (TON) of about 2.45×10^4 when t = 72 h and p_{CH4} = 125 psi. Three independent kinetic characterizations suggest that Ag^{II}-mediated CH_4 activation is kinetically favored at room temperature over the side reaction of solvent oxidation. The overall selectivity of the reaction, measured as the Faradaic efficiency (*FE*) in electrocatalysis, was observed to be 72% when p_{CH4} = 85 psi and is predicted to exceeding 99 % when p_{CH4} > 180 psi after overcoming the mass-transport constraint due to CH_4's limited solubility. The discovered reactivity of electrochemically generated Ag^{II}, in conjunction with Ag's relatively lower cost comparing to its more precious counterparts in class (b) metals (Hg notwithstanding), offer a favorable prospect for its utilization in chemical production from widely distributed natural gas with minimal infrastructure reliance.

Results and Discussion

Evidence for an electrocatalytic CH_4 functionalization

Cyclic voltammograms under various p_{CH4} values in 98% H_2SO_4 support an electrocatalytic activation of CH_4 with Ag^{I} as the pre-catalyst. Experiments of cyclic voltammetry were conducted with 5 mM Ag_2SO_4 in 98% H_2SO_4 (c_{Ag} = 10 mM), under a single-chamber three-electrode setup at 25 ºC (298 K) in a pre-defined pressure (Figure S1), with fluorine-doped tin oxide (FTO) glass as an innocent working electrode.[2a, 9d] Figure 2a shows the lack of features in voltammogram (*j-E* relationship) without the addition of Ag_2SO_4 (yellow trace). In N_2, voltammograms of Ag^{I} solution displayed an oxidative charge transfer peaking at $E_{p,a}$ = 1.82 V (all potentials are reported vs Hg_2SO_4/Hg electrode if not mentioned) before the onset of solvent oxidation at around 2.1 V (Figure 2a and 2b).[17, 19b] The corresponding reduction peak of the electrochemically generated oxidant is observed predominantly at 1.08 V, albeit a minute peak dependent on scan rate (Figure 2b and 2c) and c_{Ag} (Figure S2) is visible at 1.52 V. The reductive peak at 1.08 V is assigned as a direct reduction of Ag^{II} into Ag^{I}.[19b] The secondary one at 1.52 V is suggested as the reduction of bisulfate radicals ($HSO_4^{\bullet}$) homogenously generated from the Ag-bound bisulfate ligand (HSO_4^{-}) via a ligand-metal charge transfer (LMCT),[19b, 24] which helps explain why the integrated reductive charge is smaller than the oxidative one. We observed that the reaction kinetic responsible to the reductive peak at 1.52 V is sluggish since this peak is much less visible at a higher scan rate in Figure 2b and 2c. Despite the noted complication of reductive behavior, the single-electron oxidation peak from Ag^{I} to Ag^{II} yields a satisfactory linear relationship in the Randles-Ševčík analysis[25] (Figure 2c and 2d) with a diffusion coefficient of 2.8×10^{-7} cm^2•s^{-1}. Additional numerical simulation of cyclic voltammetry, whose details are listed in Figure S3, Table S1, and Table S2, not only

10.1002/anie.202104217

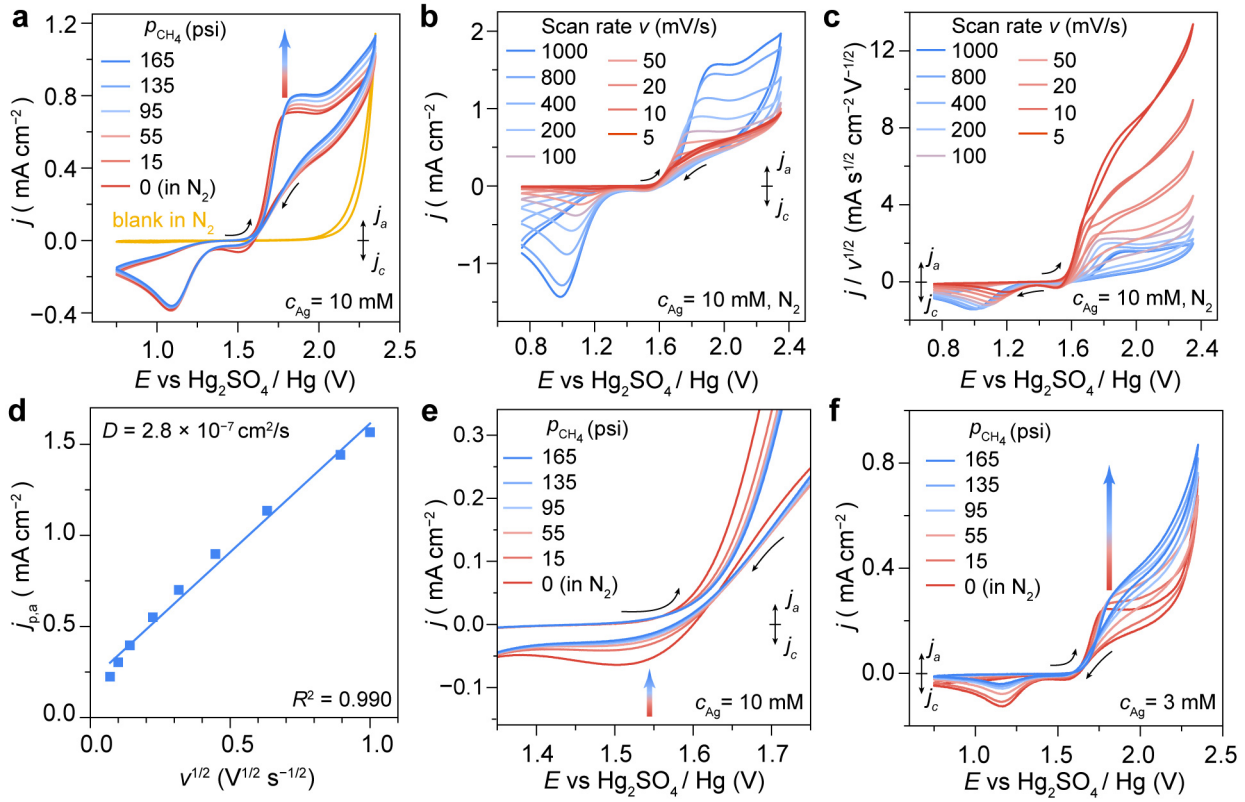

Figure 2. a) *j-E* plot when c_{Ag} = 10 mM with increasing p_{CH4} (red to blue traces) and the result without Ag in N_2 (yellow trace, "blank in N_2"). b) *j-E* plot when c_{Ag} = 10 mM in N_2 with various scan rates (v). c) $j/v^{1/2}$-E plot from results shown in (b). d) The plot of anodic peak current density ($j_{p,a}$) versus $v^{1/2}$ from results shown in (b) and (c). D, the calculated diffusion coefficient. e) Enlarged *j-E* plot in (a) at around 1.5 V. f) *j-E* relationship when c_{Ag} = 3 mM with increasing p_{CH4}. Unless noted, room temperature, 98% H_2SO_4 electrolyte, v = 100 mV·s^{-1}, and *i*R-compensated.

supports the obtained value of diffusion coefficient but also suggests a quasi-reversible electrochemical oxidation of Ag^I as a desirable *E* step in an *EC'* mechanism with a charge-transfer rate constant (k_s) of 3×10^{-6} cm/s. When the N_2 environment was switched to CH_4, a p_{CH4}-dependent change in the voltammograms was observed (Figure 2a and S4). The current density of Ag^I oxidation increases with higher p_{CH4} values, along with the decrease of reductive current density peaking at 1.08 V. In addition, a noticeable disappearance of the reductive peak at 1.52 V was observed in CH_4 (Figure 2e). As higher p_{CH4} values correlate with higher CH_4 concentrations in the electrolyte, the observed change in voltammograms is consistent with a hypothesized *EC'* mechanism mediated by electro-generated Ag^{II} (Figure 1c), in which the increased oxidative current density stems from the regenerated Ag^I near the electrode after an oxidative CH_4 activation. The disappearance of reductive peak at 1.52 V in CH_4 suggests that CH_4 competitively reacts with Ag^{II} metalloradical in lieu of LMCT on the HSO_4^- ligand, hinting the presence of a radical-based reaction pathway. We note that at room temperature CH_4 only possesses a solubility of about 0.8 mM at ambient pressure and less than 9 mM at the highest tested pressure (p_{CH4} = 165 psi, see SI), a concentration smaller than the c_{Ag} used in Figure 2a to 2e (c_{Ag} = 10 mM). This suggests mass transport of CH_4 may limit the catalytic response shown in Figure 2a. Evidently, when c_{Ag} = 3 mM, *j-E* relationship displays a more pronounced catalytic current of CH_4 activation, even at ambient pressure (15 psi) (Figure 2f). This confirms that the electrocatalytic behavior in cyclic voltammetry is limited by the solubility of CH_4 and electro-generated Ag^{II} is ambiently reactive towards CH_4.

The proposed electrocatalytic CH_4 activation is corroborated by analyzing the solution after electrolysis via ^{1}H nuclear magnetic resonance (NMR) spectroscopy. Room-temperature preparative bulk electrolysis (t = 3 h) was conducted at c_{Ag} = 10 mM in a two-chamber three-electrode setup (Figure S5), and the composition of the resultant electrolyte in the anodic chamber was analyzed by ^{1}H NMR spectroscopy. Electrolysis at E = 1.637 V and p_{CH4} = 15 psi (ambient pressure) leads to the emergence of a peak at chemical shift δ = 3.34 ppm in ^{1}H NMR spectra (blue trace in Figure 3a), consistent with a presumed formation of CH_3OSO_3H (Figure S6a). CH_3OSO_3H formation was not observed either in N_2 with Ag^I or in CH_4 devoid of Ag^I (red and yellow trace in Figure 3a, respectively). The amount of generated CH_3OSO_3H is proportional to the amount of electric charge passed and linear to t up to 12 h when E = 1.602 V (Figure 3b). This suggests that the CH_3OSO_3H production is persistent in CH_4. Attempts of detecting gas-phase products with an online gas chromatograph (Figure S1a) did not find any detectable CO, CO_2, and other carbon-based products (Figure S7). ^{13}C isotope-labeling experiment with $^{13}CH_4$ in electrolysis led to a signal at δ = 58.6 ppm in ^{13}C NMR spectrum hence $^{13}CH_3OSO_3H$ formation, which was not observable under CH_4 of natural isotope abundance (Figure 3c). Those data support an electrocatalytic

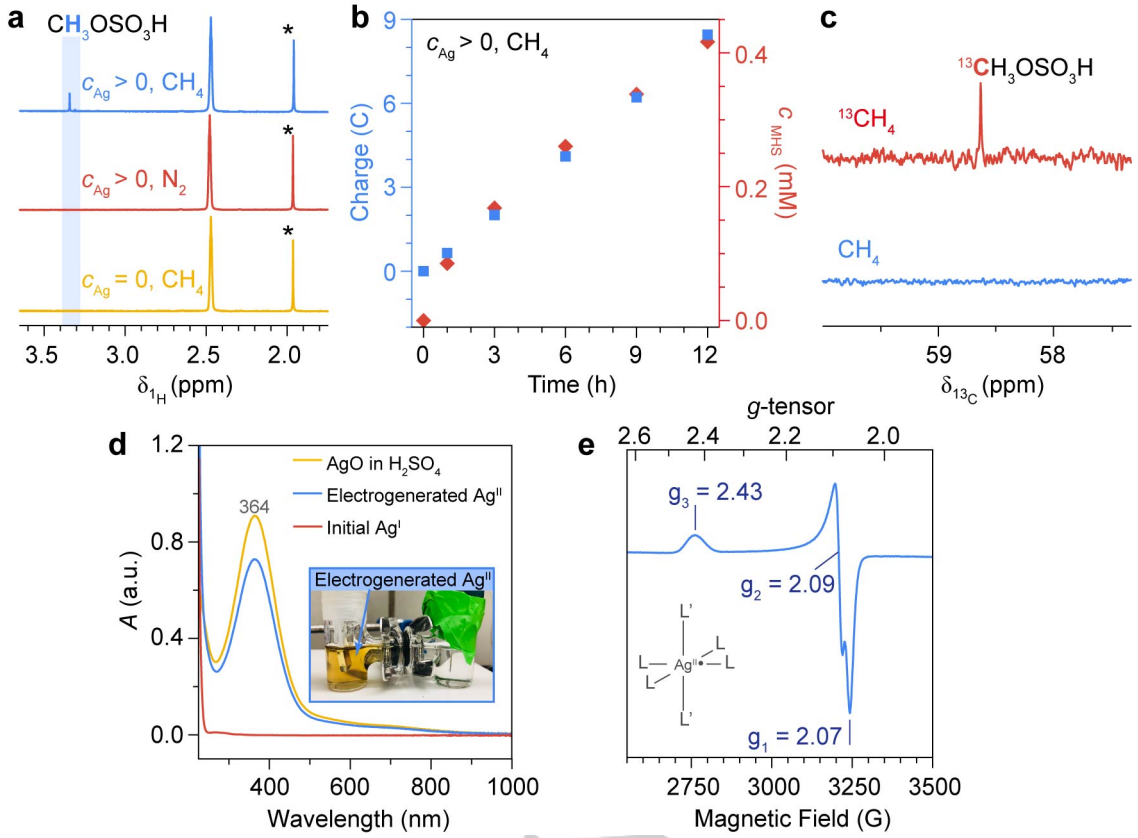

Figure 3. a) ^{1}H NMR spectra of solutions after a 3-h electrolysis with c_{Ag} = 10 mM in CH_4 (blue) and N_2 (red) or c_{Ag} = 0 mM in CH_4 (yellow). E = 1.637 V; *, Acetic acid as internal standard; d_6-DMSO. b) The evolution of electric charges (blue) and CH_3OSO_3H concentration (c_{MHS}, red) during a 12-h electrolysis. 25°C; c_{Ag} = 10 mM; E = 1.602 V. c) ^{13}C NMR spectra of solutions after a 3-h electrolysis with c_{Ag} = 3 mM in $^{13}CH_4$ (red) and CH_4 of natural abundance (blue). d_6-DMSO; E = 1.637 V. d) UV-vis spectra of the pre-catalyst Ag^{I} (red), electrogenerated Ag^{II} (blue), and AgO dissolved in 98% H_2SO_4 (yellow). The inset shows the yellow-colored electrogenerated Ag^{II}. e) EPR spectrum of AgO in 98 % H_2SO_4 (77 K).

functionalization of CH_4 into CH_3OSO_3H with minimal carbon-based side products.

Additional experimental data support a CH_4-activating electrocatalysis mediated by Ag^{II}. Visual inspection during electrolysis unveiled a yellow hue in solution near the FTO electrode under potentials anodic enough to produce Ag^{II} (insets in Figure 3d and S2), which faded away after the termination of electrochemical oxidation. UV-vis spectroscopy recorded an absorption peak at 364 nm with a shoulder around 700 nm (blue trace in Figure 3d) that existed for more than 10 min after electrolysis (Figure S8a). Such absorption features are distinct from the stable spectrum of Ag^{I} (red trace in Figure 3d) and identical to the one of commercially available AgO dissolved in 98% H_2SO_4 (yellow trace in Figure 3d and more in Figure S8b). In the solution of AgO, a distorted octahedral Ag^{II} metalloradical depicted in Figure 1c is confirmed via electron paramagnetic resonance (EPR) spectroscopy[19b, 26] with our measured spectrum at 77 K (Figure 3e; g_1 = 2.07, g_2 = 2.09, g_3 = 2.43). Given the similar optical spectra, we deemed that Ag^{II} metalloradical is generated upon electrochemical oxidation. Moreover, we found that the solution of AgO is reactive towards CH_4 ambiently and yields CH_3OSO_3H, albeit with weaker reactivity (Figure S6b). This observation supports our initial inspiration that Ag^{II} as a soft Lewis acid is reactive towards CH_4 and corroborates our proposed *EC'* mechanism mediated by Ag^{II} (Figure 1c). Last, when oleum (20% free SO_3 basis) was employed as the electrolyte, the predominant product was methanesulfonic acid (CH_3SO_3H) with a minute amount of CH_3OSO_3H (31:1 ratio) (Figure S6c). The detection of CH_3SO_3H from oleum suggests that electrolysis generates SO_3-reactive CH_3•,[7a] consistent with the implication from HSAB theory due to CH_3•'s softness (Figure 1a).

Reaction kinetics in the electrocatalysis

We evaluated the reactivity of CH_4 activation as a function of electrochemical potential E, CH_4 pressure p_{CH4}, and electrolysis duration t. When c_{Ag} = 0.5 mM and p_{CH4} = 15 psi, the partial current density (j_{CH4}) and the Faradaic efficiency (FE) of CH_3OSO_3H formation, quantified by ^{1}H NMR (Figure S6d, Table S3), are displayed against E in Figure 4a. CH_3OSO_3H formation takes place when E > 1.5 V, concurrent with Ag^{II} generation in Figure 2b. A near-plateaued j_{CH4} at higher E contributes to a maximal FE of 36.2% at 1.662 V when c_{Ag} = 0.5 mM (Figure 4a). This observed optimum of electrocatalytic CH_4 functionalization is about 600 mV more cathodic than our previously reported vanadium-oxo electrocatalyst [2a] and comparable with the Pd-based ones in literature.[9] As the observed j_{CH4} plateau does not change significantly when c_{Ag} = 10 mM (Figure S9, Table S3), it is the mass transport of CH_4 that limits both the j_{CH4} and FE since Ag^{II} seems highly reactive towards CH_4 and CH_4's solubility is about 0.8 mM ambiently (see SI).[27] Additional evaluation was conducted under elevated pressures when c_{Ag} = 0.5 (entry 1 to 4) and 3 mM (entry 5 to 10) in Figure 4b. When t = 3 h (entry 1 to 8

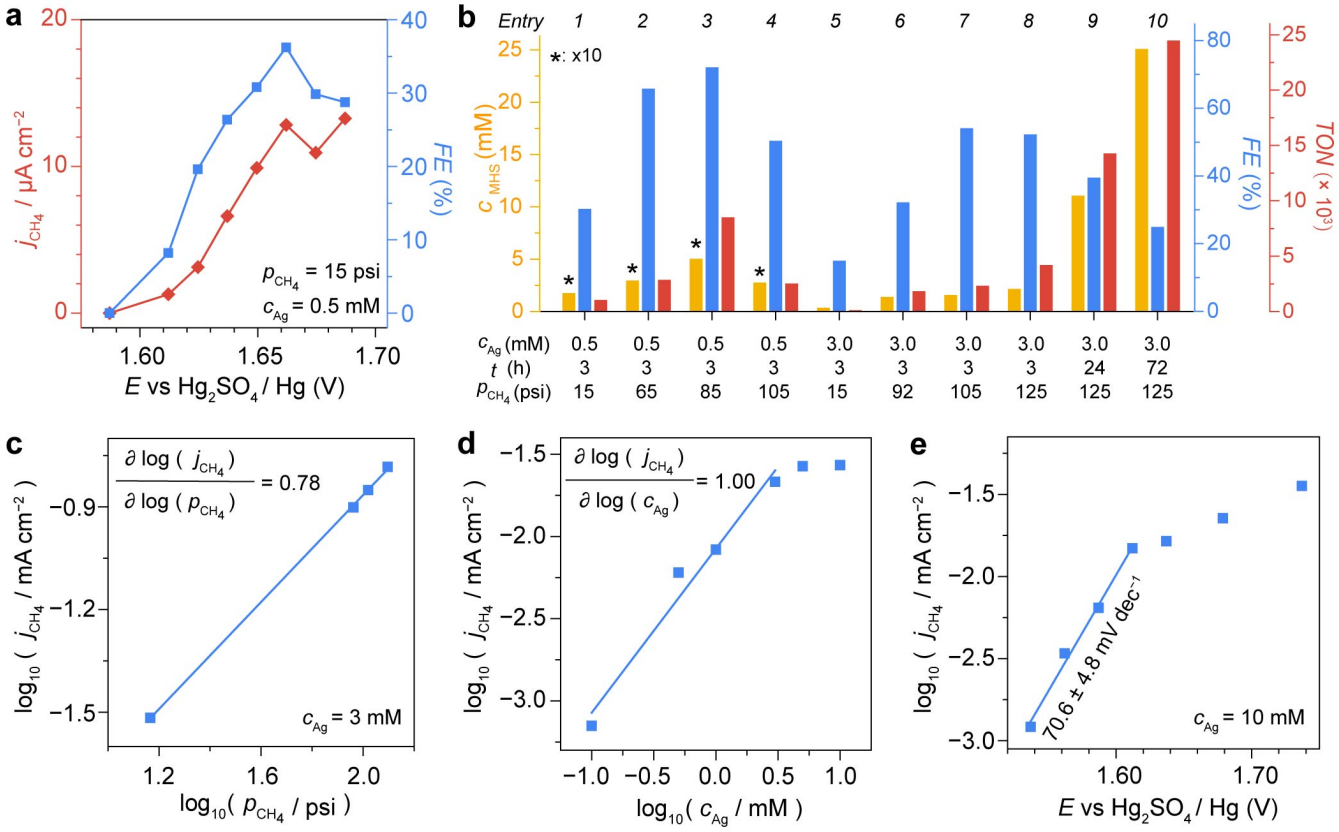

Figure 4. a) Partial current density (j_{CH4}, red) and Faradaic efficiencies (*FE*, blue) as a function of *E*. *t* = 3 h. b) Concentration of accumulated CH_3OSO_3H (c_{MHS}, yellow), *FE* (blue), and turnover numbers (TONs, red) at different values of p_{CH4}, *t*, and c_{Ag}. *E* = 1.737 V; *, Multiplied by a factor of 10. c) The plot of $\log_{10}(j_{CH4})$ versus $\log_{10}(p_{CH4})$. *E* = 1.737 V. d) The plot of $\log_{10}(j_{CH4})$ versus $\log_{10}(c_{Ag})$. p_{CH4} = 15 psi; *E* = 1.637 V. e) The plot of $\log_{10}(j_{CH4})$ versus *E*. p_{CH4} = 15 psi. Each data point is the average of at least two or three independent measurements. 25 °C.

in Figure 4b), increasing p_{CH4} leads to increased *FE* and j_{CH4} and results in a maximal *FE* of 72.1% at c_{Ag} = 0.5 mM, p_{CH4} = 85 psi, and *E* = 1.737 V (Table S4). When p_{CH4} = 15 and 85 psi, our reported data suggest a full-cell voltage of 1.07 and 1.15 V, respectively, for an electricity-driven CH_4 functionalization with the reduction O_2 into H_2O as the reduction half-reaction, in comparison to the thermodynamic driving force of 0.48 V and 0.50 V based on our calculation (Table S5). The ideal energy input, assuming a unity of *FE*, is 210 and 220 kJ mol_{CH4}^{-1} (Table S6) when p_{CH4} = 15 and 85 psi, respectively, in the context of a lower heating value (LHV) of 802 kJ mol_{CH4}^{-1} for CH_4. Comparing the results when c_{Ag} = 0.5 (entry 1 to 4) and 3 mM (entry 5 to 10) in Figure 4b, higher c_{Ag} values increase CH_3OSO_3H concentration (c_{MHS}) yet lower *FE* values, likely due to the CH_4's limited solubility. Extending *t* from 3 h to 72 h yielded c_{MHS} > 25 mM when c_{Ag} = 3 mM (25 ºC, p_{CH4} = 125 psi, and *E* = 1.737 V; entry 9 and 10 in Figure 4b, S10, and Table S7). While there remains much room for optimization, the reported values of *FE* and c_{MHS} illustrate the favorable intrinsic activity and practical usability of this ambient electrocatalytic CH_4 activation.

Electrocatalytic kinetics was determined to be first-order on both CH_4 and Ag^{II} with a turnover-limiting CH_4 activation and a high value of pseudo-first-order rate constant k_{obs}. Devoid of mass-transport complication, j_{CH4} as a surrogate of the CH_4-activation rate is found to be mostly linear with p_{CH4}. When c_{Ag} = 3 mM and *E* = 1.737 V, $\partial\log_{10}(j_{CH4})/\partial\log_{10}(p_{CH4})$ = 0.78 (Figure 4c, Table S4). Experiments with c_{Ag} as a proxy of electrogenerated Ag^{II} yielded $\partial\log_{10}(j_{CH4})/\partial\log_{10}(c_{Ag})$ = 1.00 when p_{CH4} = 15 psi and *E* = 1.637 V (Figure 4d, Table S8). Those results suggest that the turnover-limiting step probably involves one equivalent of CH_4 and Ag^{II}. Plotting $\log_{10}(j_{CH4})$ versus *E* when c_{Ag} = 10 mM and p_{CH4} = 15 psi yielded a Tafel slope of 70.6±4.8 mV/dec (Figure 4e, Table S3). The obtained value of Tafel slope is in accordance with a proposed *EC'* mechanism with a continuous regeneration of Ag^{II} (*E* step) and a turnover-limiting CH_4-activating *C'* step (Figure 1c), which predicts a theoretical value of 60 mV/dec for Tafel slope.[28] The obtained reaction kinetics on Ag enables us to calculate $k_{obs,b}$ as the pseudo-first-order rate constant of CH_4 activation,[29] frequently dubbed as turnover frequency, based on bulk electrolysis data (hence the subscript "b").[2a, 30] At 25 ºC, c_{Ag} = 0.5 mM, and *E* = 1.737 V, $k_{obs,b}$ reaches as high as 3.5×10^2 and 2.8×10^3 h^{-1} when p_{CH4} = 15 and 85 psi, respectively (Table S4). The values of $k_{obs,b}$ are on par with some of the best electrocatalysts for CH_4 activation (Table S9).[2a, 9d, 11c] Furthermore, we calculated the effective turnover number (TON) of CH_4 activation, presented in Figure 4b. [30a, 30b] Similarly due to CH_4's limited solubility (vide supra), higher c_{Ag} yielded lower TON when comparing between c_{Ag} = 0.5 (entry 1 to 4) and 3 mM (entry 5 to 10) in Figure 4b. Prolonged electrolysis increases the calculated TON values. When *t* = 72 h and p_{CH4} = 125 psi, TON tops 2.45×10^4 (entry 10 in Figure 4b, Table S7) and no intrinsic issue seems to prevent the electrocatalytic system from keeping operation. The obtained TON value showcases the longevity of the discovered electrocatalyst.

10.1002/anie.202104217

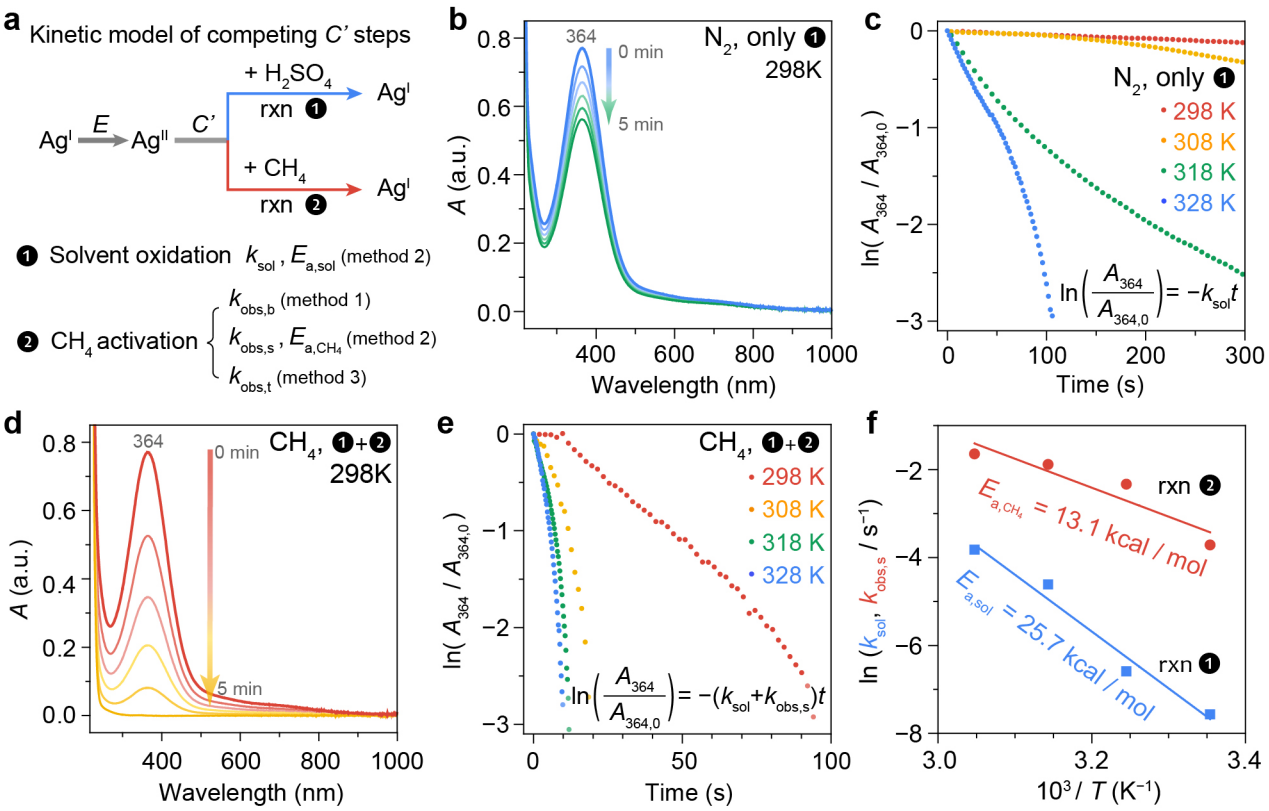

Figure 5. a) A kinetic model that includes competing Ag^{II}-based solvent oxidation (❶) and CH_4 activation (❷), which were studied via steady-state bulk electrolysis ("method 1"), temperature-dependent UV-vis absorption spectroscopy ("method 2"), and double potential step chronoamperometry ("method 3"). (b to e) The time evolutions of Ag^{II}'s absorption spectra at 298 K (b, d) and the logarithmic of normalized absorbance at 364 nm $\ln(A_{364}/A_{364,0})$ under different temperatures (c, e) when p_{CH4} = 0 (b, c) and 15 psi (d, e). f) The logarithmic of pseudo-first-order rate constant for solvent oxidation ($\ln(k_{sol})$, blue) and CH_4 activation ($\ln(k_{obs,s})$, red) versus the inverse of temperature (1/*T*). $E_{a,sol}$ and $E_{a,CH4}$, the calculated activation energies for Ag^{II}-based solvent oxidation and CH_4 activation, respectively.

We found that CH_4 activation is kinetically favored over the undesirable side reaction of solvent oxidation. In 98% H_2SO_4 electrogenerated Ag^{II} either activates CH_4 or reacts with solvent possibly via a $HSO_4^{\bullet}$-yielding LMCT (vide supra). We quantitatively established a reaction model that includes two competing reaction pathways: CH_4 activation and the undesirable solvent oxidation (Figure 5a). The $k_{obs,b}$ calculated from bulk electrolysis offers the first approach for elucidating the kinetics of CH_4 activation branch ("method 1" in Figure 5a). We also took advantages of the difference in optical absorption between Ag^{I} and Ag^{II} (Figure 3d and S2) and the equivalent identity of Ag^{II} in the AgO solution and the post-electrolyzed Ag^{I} solution (Figure S8, vide supra), and henceforth employed the Ag^{II}'s absorbance at 364 nm (A_{364}) of AgO solution to probe the transient of Ag^{II} at different temperatures ("method 2" in Figure 5a, see SI). When p_{CH4} = 0 psi, the initial decrease of A_{364} from Ag^{II} followed a first-order kinetics for solvent oxidation (Figure 5b and 5c), which possesses a rate constant k_{sol} = 1.9 h^{-1} at 25 ºC and an activation energy $E_{a,sol}$ = 25.7 kcal/mol (Figure 5f, Table S10). When p_{CH4} = 15 psi, the initial A_{364} decrease contributed from both solvent oxidation and CH_4 activation similarly followed a first-order kinetics and was much faster (Figure 5d and 5e). The resultant pseudo-first-order rate constant of CH_4 activation from absorption spectroscopy (hence the subscript "s") $k_{obs,s}$ = 88 h^{-1} at 25 ºC with an activation energy $E_{a,CH4}$ = 13.1 kcal/mol (Figure 5f, Table S10). Furthermore, although our setup of UV-vis absorption spectroscopy is unable to operate at elevated pressure, experiments of double potential step chronoamperometry[28] at higher values of p_{CH4} indicate that k_{obs} is linearly dependent on p_{CH4} ("method 3" in Figure 5a). At a certain p_{CH4} value, *E* was first poised at 2.0 V to oxidatively generate Ag^{II} population near the electrode; then *E* was switched to 0.75 V at which potential the residual Ag^{II} that had not reacted was reduced back to Ag^{I}. Right after the potential application of 2.0 V on the electrode, current density *j* was recorded under different p_{CH4} (Figure 6a). Qualitatively, the higher steady-state *j*(t) under higher p_{CH4} at 2.0 V indicates a CH_4-mediated electrocatalysis while the constant steady-state *j*(t) at 0.75 V suggests that a Ag-based catalytic cycle imposes no loss of Ag in the solution. If $j_0(t)$ is denoted as the transient $j(t)$ value when p_{CH4} = 0 psi, $k_{obs,t}$ based on such transient measurement (hence the subscript "t") can be mathematically described:

$$\frac{j(t)}{j_0(t)} = \sqrt{\pi k_{obs,t} t} \qquad (1)$$

The plots of $j(t)/j_0(t)$ versus $t^{1/2}$ at various p_{CH4} values are displayed in Figure 6b and the calculated $k_{obs,t}$ values are mostly linear to p_{CH4} (Figure 6c, Table S11). The slope of $k_{obs,t}$ versus p_{CH4}, at a value of 2.8×10^{-4} $psi^{-1}\cdot s^{-1}$, yields k_{cat} as the second-order rate constant of the bimolecular reaction between Ag^{II} and CH_4. The observed linear relationship between $k_{obs,t}$ and p_{CH4} offers another evidence that the Ag^{II}-based CH_4 activation is the turnover-limiting step. Overall, the rate constants of Ag^{II}-based CH_4 activation were determined via three independent methods (Figure 5a): steady-state bulk electrolysis ($k_{obs,b}$), time-dependent absorption

10.1002/anie.202104217

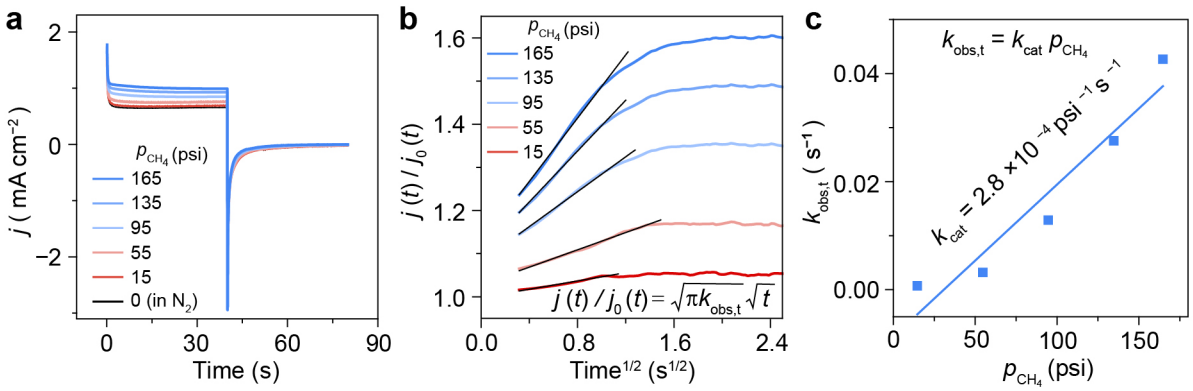

Figure 6. a) Double potential step chronoamperometry at different p_{CH4}. E = 2.0 and 0.75 V for time $t \in$ [0, 40 s] and $t \in$ [40 s, 80 s], respectively; c_{Ag} = 10 mM. b) The plot of $j(t)/j_0(t)$ versus $t^{1/2}$ based on the results in (a) at different p_{CH4}. $j_0(t)$ and $j(t)$, current densities at time t when p_{CH4} = 0 and $p_{CH4} \neq 0$, respectively. c) Pseudo-first-order rate constant $k_{obs,t}$ for CH_4 activation extracted from the linear region in (b) as a function of p_{CH4}.

spectroscopy ($k_{obs,s}$), and double potential step chronoamperometry ($k_{obs,t}$). Notwithstanding the values of $k_{obs,s}$ fetched when c_{Ag} > 10 mM, a satisfactory agreement was reached at low c_{Ag} value (Table S12). The larger rate constant and the lower value of activation energy for CH_4 activation suggest that during ambient electrocatalysis CH_4 functionalization is order-of-magnitude faster than the undesirable solvent oxidation.

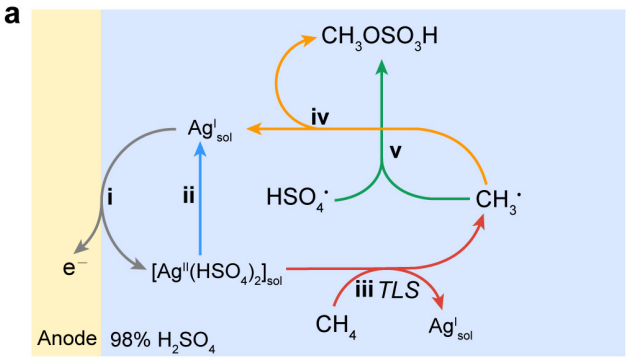

b

***E* step:** Electrochemical generation of Ag^{II}

i $Ag^I_{sol} + 4/3\ H_2SO_4 + 2/3\ HSO_4^- \longrightarrow [Ag^{II}(HSO_4)_2]_{sol} + 4/3\ H^+ + e^-$

Side reaction: Solvent oxidation

ii $[Ag^{II}(HSO_4)_2]_{sol} \longrightarrow Ag^I_{sol} + HSO_4^{\bullet} + HSO_4^-$

$E_{a,sol}$ = 25.7 kcal/mol

***C'* step:** CH_4 functionalization

iii *TLS* $[Ag^{II}(HSO_4)_2]_{sol} + CH_4 \longrightarrow Ag^I_{sol} + CH_3^{\bullet} + H_2SO_4 + HSO_4^-$

iv $[Ag^{II}(HSO_4)_2]_{sol} + CH_3^{\bullet} \longrightarrow Ag^I_{sol} + CH_3OSO_3H + HSO_4^-$

v $HSO_4^{\bullet} + CH_3^{\bullet} \longrightarrow CH_3OSO_3H$

C' step (iii + iv)

$2\ [Ag^{II}(HSO_4)_2]_{sol} + CH_4 \longrightarrow 2\ Ag^I_{sol} + CH_3OSO_3H + H_2SO_4 + 2\ HSO_4^-$

E_{a,CH_4} = 13.1 kcal/mol

Overall electrocatalytic oxidation: i × 2 + (iii + iv)

$$CH_4 + H_2SO_4 \xrightarrow[98\ \%\ H_2SO_4]{Ag\ cat.,\ 25\ ^\circ C} CH_3OSO_3H + 2\ H^+ + 2\ e^-$$

Figure 7. a) A proposed catalytic cycle. b) Individual steps **i** to **v** in the catalysis and the overall electrocatalytic oxidation reaction. *TLS*, turnover-limiting step.

Reaction mechanism and attainable Faradaic efficiency

Our results warrant a mechanistic discussion in this electrocatalytic CH_4 activation inspired by HSAB theory (Figure 7). We showed that an electrochemical oxidation of Ag^I yields Ag^{II} metalloradical continuously (*E* step and route **i** in Figure 7). EPR spectroscopy supports Ag^{II}'s radical nature and the quasi-reversible oxidative charge transfer is supported by the successful application of Randles-Ševčík analysis and numerical simulation.[25] Without CH_4, Ag^{II} slowly undergoes solvent oxidation (route **ii** in Figure 7; k_{sol} = 1.9 h^{-1} and $E_{a,sol}$ = 25.7 kcal/mol at 25 ºC), possibly via a $HSO_4^{\bullet}$-yielding LMCT[19b, 31] as evident in the reductive peak of 1.52 V in the cyclic voltammogram. The resultant $HSO_4^{\bullet}$ is proposed to further dimerize and yield persulfate, which eventually can disproportionate and generate O_2 (Figure S11).[19b, 32] In CH_4, a turnover-limiting reaction between one equivalent of Ag^{II} and CH_4 initiates CH_4 activation (route **iii** in Figure 7). The first-order reaction kinetics for both Ag^{II} and CH_4 has been supported by the near-unity values of $\partial\log_{10}(j_{CH4})/\partial\log_{10}(p_{CH4})$ and $\partial\log_{10}(j_{CH4})/\partial\log_{10}(c_{Ag})$ in bulk electrolysis, the time-dependent change of A_{364} for Ag^{II}, and the experiments of double potential step chronoamperometry. The reported pseudo-first-order rate constant k_{obs} = 3.5×10² or 88 h^{-1} ($k_{obs,b}$ and $k_{obs,s}$, respectively) at 25 ºC and p_{CH4} = 15 psi with $E_{a,CH4}$ = 13.1 kcal/mol. The quantitative determination of reaction kinetics offers opportunities for additional understanding and design of the reported electrocatalytic system.

We pondered whether Ag^{II} is directly responsible to turnover-limiting C−H activation in CH_4 (*C'* step and route **iii** in Figure 7) and the nature of reactions after CH_4 activation during catalysis (route **iv** and **v** in Figure 7). We contend that $HSO_4^{\bullet}$ generated from the LMCT of Ag-bound HSO_4^- has a minimal contribution, if any, in the turnover-limiting step of Ag^{II}-initiated CH_4 activation, not only because the inclusion of $HSO_4^{\bullet}$ will prevent a first-order kinetics for both Ag^{II} and CH_4 but also because $HSO_4^{\bullet}$ thermally generated from persulfate is reported as inactive towards CH_4.[2a, 9b] The electrolysis in oleum with yielded CH_3SO_3H suggests the presence of CH_3• intermediate.[7a] As η = 6.7, 6.42, and 4.87 for Ag^{II}, H•, and CH_3•, respectively,[5] we postulate a homolytic CH_4 cleavage in the turnover-limiting step, while we do not exclude the possibility of a Ag−CH_3 intermediate from electrophilic activation. The reaction steps after the turnover-limiting step of CH_4 activation remain elusive. We tentatively consider that the yielded CH_3• can either directly react

with another Ag^{II} for a consecutive two-electron oxidation (route **iv** in Figure 7), or react with one $HSO_4^{\bullet}$ indirectly generated from Ag^{II} to yield CH_3OSO_3H (route **v** in Figure 7). Nonetheless, as shown by our data, the branch of CH_4-activating pathway is kinetically faster than the solvent oxidation at room temperature and ambient pressure, paving a selective electrocatalytic CH_4 activation. Assuming two consecutive Ag^{II}-mediated oxidations for one equivalent of CH_4 activation (route **iii** and **iv** in Figure 7), the half-reaction of overall electrocatalysis is written as:

$$CH_4\,(g) + H_2SO_4\,(l) \xrightarrow{ambient} CH_3OSO_3H\,(l) + 2\,H^+\,(solvated) + 2\,e^- \qquad (2)$$

Last, the quantification of reaction kinetics indulges us to predict the electrocatalysis's ultimate performance when all of the engineering constraints, particularly the mass transport of CH_4, are successfully addressed in a hypothetical scenario. In particular, we are interested in the *FE* towards CH_4 functionalization. Our established kinetic model (Figure 5 and 6) suggests that the pseudo-first-order kinetic rate constant of CH_4 activation and the selectivity towards CH_4 activation are both functions of CH_4 pressure p_{CH4} and temperature T, i.e. $k_{obs} = k_{obs}(p_{CH4}, T)$ and $FE = FE(p_{CH4}, T)$. We utilized our kinetic model shown in Figure 5a and calculated the values of $FE(p_{CH4}, T)$ as a function of p_{CH4} and T (Figure 8, Table S13):

$$FE(p_{CH4}, T) = \frac{k_{obs,t}(p_{CH4}, 298)e^{-\frac{E_{a,CH4}}{R}\left(\frac{1}{T}-\frac{1}{298}\right)}}{k_{obs,t}(p_{CH4}, 298)e^{-\frac{E_{a,CH4}}{R}\left(\frac{1}{T}-\frac{1}{298}\right)} + k_{sol}(298)e^{-\frac{E_{a,sol}}{R}\left(\frac{1}{T}-\frac{1}{298}\right)}} \qquad (3)$$

At T = 25 ºC (298K), $FE(p_{CH4}, T)$ is calculated as 53% at ambient pressure (p_{CH4} = 15 psi). *FE* reaches 90% when p_{CH4} > 62 psi (4.3 bar), 95% when p_{CH4} > 85 psi (5.9 bar), and 99% when p_{CH4} > 180 psi (12.4 bar) (Figure 8). This suggests that Ag-based electrocatalysis of CH_4 activation is capable of reaching near-unity selectivity at room temperature and an accessible p_{CH4} that is much lower than the syngas synthesis from steam reforming of CH_4 (650 ºC and 30 bar).[33] We also considered how reaction temperature T affects *FE* (Figure 8). *FE* drops significantly at higher temperature, because $E_{a,sol} > E_{a,CH4}$ and hence the rate of solvent oxidation increases much faster than the one of CH_4 activation. This suggests that Ag^{II}-mediated electrocatalysis is selective and specifically suitable at lower temperature. While the absolute rate of CH_4 activation increases with temperature, it is the competition between CH_4 activation and the undesirable solvent oxidation that dictates the selectivity. Overall, calculations of $FE(p_{CH4}, T)$ suggest that the Ag^{II}-mediated electrocatalysis is reactive and selective for low-temperature CH_4 functionalization and further engineering optimization will be constructive to reach the electrocatalyst's full potential.

Conclusion

Inspired by the HSAB theory, we explored the electrocatalytic CH_4 functionalization mediated by Ag^{II} metalloradical, the last class (b) metal whose reactivity towards CH_4 is unknown. Kinetic characterization establishes that selective electrocatalytic CH_4 activation proceeds ambiently in 98% H_2SO_4 with low activation energy and high kinetic rate constant. The electrocatalytic system is unique that low reaction temperature is preferred for high reaction selectivity, while a reaction pressure slightly higher than ambience (6~10 bar) favors the overall turnover. Future experiments are desired to continue investigating the nature of reactions after the turnover-limiting CH_4 activation. Engineering optimization is needed to overcome the mass transport limitation due to CH_4 limited solubility and maximize the electrocatalysis's selectivity at low temperature. Moreover, the successful inquiry of CH_4 catalysts initiated based on the chemical hardness of possible reaction intermediates encourages us to adopt such a strategy to discover more CH_4-activating catalysts, particularly with electrochemical charge transfer as the reaction's driving force. This work offers a new route of ambient electrocatalytic CH_4 functionalization as well as a strategy that may be generally applicable for future catalyst design, in order to achieve chemical production from widely distributed natural gas resources with minimal infrastructure reliance.

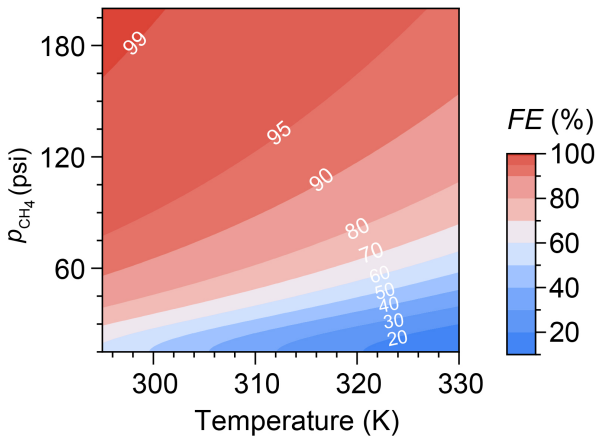

Figure 8. Calculated *FE* as a function of p_{CH4} and T based on the established kinetic model and the measured kinetic parameters.

Notes

A provisional patent has been filed under the names of C.L., D.X., J.A.I., J.D.. All other authors declare no competing interests.

Acknowledgements

We thank Dr. Paul Oyala at Caltech for the use of the EPR spectrometer and Prof. Dr. Ellen Sletten at UCLA for the use of temperature-dependent UV-vis spectrophotometer. We thank Dr. Di Yang and Dr. Shengtao Lu for helpful discussions, and Mr. Gary Chan for setup preparation. We thank the Molecular Instrumentation Center lab at UCLA for sample characterizations. J.A.I. acknowledges a Eugene V. Cota-Robles Fellowship. C.L. acknowledges the NSF Award (CHE-1955836), startup fund from UCLA, and the financial support of the Jeffery and Helo Zink Endowed Professional Development Term Chair.

Keywords: electrochemistry • high-valent silver • homogeneous catalysis • HSAB theory • methane functionalization

[1] a) D. Malakoff, *Science* **2014**, *344*, 1464-1467; b) O. Edenhofer, R. Pichs-Madruga, Y. Sokona, J. C. Minx, E. Farahani, K. Susanne, K. Seyboth, A. Adler, I. Baum, S. Brunner, P. Eickemeier, B. Kriemann, J. Savolainen, S. Schlomer, C. von Stechow, T. Zwickel, *Working Group III Contribution to the Fifth Assessment Report of the Intergovernmental Panel on Climate Change, Climate Change 2014: Mitigation of Climate Change*, Cambridge University Press, **2015**; c) J. F. Hartwig, *J. Am. Chem. Soc.* **2016**, *138*, 2-24.

[2] a) J. Deng, S.-C. Lin, J. Fuller, J. A. Iñiguez, D. Xiang, D. Yang, G. Chan, H. M. Chen, A. N. Alexandrova, C. Liu, *Nat. Commun.* **2020**, *11*, 3686; b) N. J. Gunsalus, A. Koppaka, S. H. Park, S. M. Bischof, B. G. Hashiguchi, R. A. Periana, *Chem. Rev.* **2017**, *117*, 8521-8573; c) X. Meng, X. Cui, N. P. Rajan, L. Yu, D. Deng, X. Bao, *Chem* **2019**, *5*, 2296-2325.

[3] R. G. Parr, R. G. Pearson, *J. Am. Chem. Soc.* **1983**, *105*, 7512-7516.

[4] R. G. Parr, L. v. Szentpály, S. Liu, *J. Am. Chem. Soc.* **1999**, *121*, 1922-1924.

[5] R. G. Pearson, *Inorg. Chem.* **1988**, *27*, 734-740.

[6] a) R. A. Periana, D. J. Taube, H. Taube, E. R. Evitt (Catalytica, Inc.), U.S. Patent 5,306,855, **1994**; b) R. A. Periana, D. J. Taube, E. R. Evitt, D. G. Löffler, P. R. Wentrcek, G. Voss, T. Masuda, *Science* **1993**, *259*, 340-343; c) B. G. Hashiguchi, M. M. Konnick, S. M. Bischof, S. J. Gustafson, D. Devarajan, N. Gunsalus, D. H. Ess, R. A. Periana, *Science* **2014**, *343*, 1232-1237.

[7] a) N. Basickes, T. E. Hogan, A. Sen, *J. Am. Chem. Soc.* **1996**, *118*, 13111-13112; b) A. E. Sherry, B. B. Wayland, *J. Am. Chem. Soc.* **1990**, *112*, 1259-1261.

[8] a) X. X. Zhang, B. B. Wayland, *J. Am. Chem. Soc.* **1994**, *116*, 7897-7898; b) M. Lin, A. Sen, *Nature* **1994**, *368*, 613-615.

[9] a) R. A. Periana, O. Mironov, D. Taube, G. Bhalla, C. J. Jones, *Science* **2003**, *301*, 814-818; b) R. S. Kim, A. Nazemi, T. R. Cundari, Y. Surendranath, *ACS Catal.* **2020**, *10*, 14782-14792; c) R. S. Kim, E. C. Wegener, M. C. Yang, M. E. O'Reilly, S. Oh, C. H. Hendon, J. T. Miller, Y. Surendranath, *J. Am. Chem. Soc.* **2020**, *142*, 20631-20639; d) M. E. O'Reilly, R. S. Kim, S. Oh, Y. Surendranath, *ACS Cent. Sci.* **2017**, *3*, 1174-1179.

[10] K. J. H. Young, J. Oxgaard, D. H. Ess, S. K. Meier, T. Stewart, I. I. I. W. A. Goddard, R. A. Periana, *Chem. Commun.* **2009**, 3270-3272.

[11] a) R. A. Periana, D. J. Taube, S. Gamble, H. Taube, T. Satoh, H. Fujii, *Science* **1998**, *280*, 560-564; b) O. A. Mironov, S. M. Bischof, M. M. Konnick, B. G. Hashiguchi, V. R. Ziatdinov, W. A. Goddard, M. Ahlquist, R. A. Periana, *J. Am. Chem. Soc.* **2013**, *135*, 14644-14658; c) R. S. Kim, Y. Surendranath, *ACS Cent. Sci.* **2019**, *5*, 1179-1186.

[12] a) G. B. Shul'pin, A. E. Shilov, G. Süss-Fink, *Tetrahedron Lett.* **2001**, *42*, 7253-7256; b) C. J. Jones, D. Taube, V. R. Ziatdinov, R. A. Periana, R. J. Nielsen, J. Oxgaard, W. A. Goddard III, *Angew. Chem. Int. Ed.* **2004**, *43*, 4626-4629; *Angew. Chem.* **2004**, *116*, 4726-4729.

[13] M. N. Vargaftik, I. P. Stolarov, I. I. Moiseev, *J. Chem. Soc., Chem. Commun.* **1990**, 1049-1050.

[14] a) M. Drees, T. Strassner, *J. Org. Chem.* **2006**, *71*, 1755-1760; b) M. D. Khokhar, R. S. Shukla, R. V. Jasra, *J. Mol. Catal. A: Chem.* **2009**, *299*, 108-116.

[15] a) T. Osako, E. J. Watson, A. Dehestani, B. C. Bales, J. M. Mayer, *Angew. Chem. Int. Ed.* **2006**, *45*, 7433-7436; *Angew. Chem.* **2006**, *118*, 7593-7596; b) Q. Yuan, W. Deng, Q. Zhang, Y. Wang, *Adv. Synth. Catal.* **2007**, *349*, 1199-1209.

[16] W. M. Haynes, *CRC Handbook of Chemistry and Physics*, 97th ed., CRC Press/Taylor & Francis, Boca Raton, Florida, **2016**.

[17] P. Połczyński, R. Jurczakowski, W. Grochala, *Chem. Commun.* **2013**, *49*, 7480-7482.

[18] a) P. Xu, S. Guo, L. Wang, P. Tang, *Angew. Chem. Int. Ed.* **2014**, *53*, 5955-5958; *Angew. Chem.* **2014**, *126*, 6065-6068; b) Q.-Z. Zheng, N. Jiao, *Chem. Soc. Rev.* **2016**, *45*, 4590-4627; c) P. Leszczynski, A. K. Budniak, W. M. Adamczyk, J. H. Gawrackzynski, T. E. Gilewski, P. Polyczynski, R. R. Jurczakowski, W. R. Grochala, Z. Mazej (University of Warsaw), WO 2017/042624 Al, **2017**.

[19] a) W. Grochala, *Phys. Status. Solidi. B* **2006**, *243*, R81-R83; b) P. Połczyński, R. Jurczakowski, W. Grochala, *J. Phys. Chem. C* **2013**, *117*, 20689-20696.

[20] a) N. Sauermann, T. H. Meyer, Y. Qiu, L. Ackermann, *ACS Catal.* **2018**, *8*, 7086-7103; b) C. Ma, P. Fang, T.-S. Mei, *ACS Catal.* **2018**, *8*, 7179-7189.

[21] P. Połczyński, T. E. Gilewski, J. Gawraczyński, M. Derzsi, P. J. Leszczyński, W. Gadomski, Z. Mazej, R. Jurczakowski, W. Grochala, *Eur. J. Inorg. Chem.* **2016**, *2016*, 5401-5404.

[22] B. S. Natinsky, S. Lu, E. D. Copeland, J. C. Quintana, C. Liu, *ACS Cent. Sci.* **2019**, *5*, 1584-1590.

[23] E. S. Rountree, B. D. McCarthy, T. T. Eisenhart, J. L. Dempsey, *Inorg. Chem.* **2014**, *53*, 9983-10002.

[24] a) W. Grochala, *J. Fluorine Chem.* **2008**, *129*, 82-90; b) P. J. Malinowski, M. Derzsi, Z. Mazej, Z. Jagličić, B. Gaweł, W. Łasocha, W. Grochala, *Angew. Chem. Int. Ed.* **2010**, *49*, 1683-1686; *Angew. Chem.* **2010**, *122*, 1727-1730; c) W. Grochala, *J. Supercond. Nov. Magn.* **2018**, *31*, 737-752.

[25] N. Elgrishi, K. J. Rountree, B. D. McCarthy, E. S. Rountree, T. T. Eisenhart, J. L. Dempsey, *J. Chem. Edu.* **2018**, *95*, 197-206.

[26] A. Abragam, B. Bleaney, *Electron Paramagnetic Resonance of Transition Ions*, OUP, Oxford, **2012**.

[27] A. Sen, M. A. Benvenuto, M. Lin, A. C. Hutson, N. Basickes, *J. Am. Chem. Soc.* **1994**, *116*, 998-1003.

[28] J. B. Allen, R. F. Larry, *Electrochemical Methods: Fundamentals and Applications*, 2nd ed., John Wiley & Sons, **2001**.

[29] S. J. Meek, C. L. Pitman, A. J. M. Miller, *J. Chem. Edu.* **2016**, *93*, 275-286.

[30] a) C. Costentin, S. Drouet, M. Robert, J.-M. Savéant, *J. Am. Chem. Soc.* **2012**, *134*, 11235-11242; b) J.-M. Savéant, *Elements of Molecular and Biomolecular Electrochemistry*, J. Wiley & Sons, Inc., Hoboken, NJ, **2006**; c) C. Tsay, J. Y. Yang, *J. Am. Chem. Soc.* **2016**, *138*, 14174-14177.

[31] W. Grochala, Z. Mazej, *Phil. Trans. R. Soc. A.* **2015**, *373*, 20140179.

[32] a) J. E. House, K. A. House, in *Descriptive Inorganic Chemistry*, 3rd ed., Academic Press, Boston, **2016**, pp. 245-268; b) J. Zhu, K. K. Hii, K. Hellgardt, *ACS Sustainable Chem. Eng.* **2016**, *4*, 2027-2036; c) I. M. Kolthoff, I. K. Miller, *J. Am. Chem. Soc.* **1951**, *73*, 3055-3059.

[33] J. Rostrup-Nielsen, L. J. Christiansen, *Concepts in Syngas Manufacture*, Imperial College Press, **2011**.

10.1002/anie.202104217

Entry for the Table of Contents

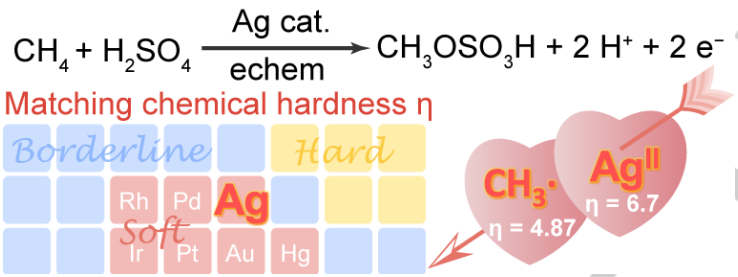

Inspired by the HSAB theory, we explored the electrocatalytic CH_4 functionalization mediated by Ag^{II} metalloradical, the last class (b) transition metal whose reactivity towards CH_4 is unknown. Detailed mechanistic investigation unveils a low activation energy of 13.1 kcal•mol^{-1} and a high pseudo-first-order rate constant of CH_4 activation up to 2.8×10^3 h^{-1} at room temperature.